DOI: 10.61782/fa.2025.0017

FORUM ACUSTICUM EURONOISE 2025

A METHOD FOR MEASURING INSTANTANEOUS STRUCTURAL INTENSITY IN FLAT STRUCTURES

Keisuke Abe[1, 2*] **Hironori Yamada**[1] **Toru Yamazaki**[2]

[1] SUBARU Corporation, 1-1, Subaru-cho, Ota-shi, Gunma, Japan
[2] Kanagawa University, 3-27-1 Rokukakubashi, Kanagawa-ku, Yokohama-shi, Kanagawa, Japan

ABSTRACT

We propose a method for measuring instantaneous structural intensity (SI) in flat structures using finite difference approximations. Based on flat plate theory, stress components associated with bending moments, torsional moments, and shear forces are described in terms of vibration displacement. The derivation formulation is established by applying finite difference approximations to partial differential terms up to fourth order in both time and space. To achieve high temporal and spatial resolution, vibration displacement is measured non-invasively using a Laser Doppler Vibrometer (LDV). This approach ensures precision and avoids contact-induced measurement errors. The proposed method demonstrated strong correlation with finite element method (FEM) simulations, confirming its validity and practicality for analyzing instantaneous SI.

Keywords: *Road noise, structural intensity, Finite Difference Method (FDM), Laser Doppler Vibrometer (LDV)*

[*] ***Corresponding author***: *abe.keisuke@subaru.co.jp*

1. INTRODUCTION

Structure-borne noise, such as road noise, is primarily radiated from the out-of-plane vibrations of vehicle body panels. Therefore, understanding the vibration transmission path from the input point to the panel is essential for noise reduction. One method for evaluating this transmission is structural intensity (SI), which represents the vibrational energy flow within a structure as a vector quantity [1].

The wave solution of SI is expressed as the squared difference between the amplitudes of the forward and backward waves [2]. The authors focused on the early-stage propagating wave, where the forward wave is dominant (hereafter referred to as the "first wave") and proposed an evaluation method for its vibrational energy flow in terms of instantaneous SI. Finite element method (FEM) simulations demonstrated that controlling instantaneous SI can effectively reduce structural responses [3]. Additionally, since the propagation characteristics of the first wave are primarily governed by the structural geometry and material properties—rather than frequency—it is expected that first-wave control can contribute to broadband noise reduction [4-5].

Since Pavić first proposed an SI measurement method using finite difference approximation [6], numerous studies have been reported on SI evaluation under steady-state conditions [7-8]. However, research on time-series evaluations of vibrational energy flow under transient conditions is limited, and to the best of our knowledge, no studies have been reported on measuring SI focusing specifically on the first-wave propagation.

Measuring instantaneous SI in the first-wave regime presents two major challenges. First, road noise typically spans a frequency range of approximately 100 Hz to 1 kHz, where

the short wavelengths and high propagation speeds necessitate high temporal and spatial resolution in measurement. Traditional physical sensors such as MEMS or accelerometer arrays suffer from phase errors, resolution limitations, mass loading effects, and manual installation errors, making multi-point measurement both challenging and labor-intensive [9]. Second, since the first wave propagating through the medium is dominated by fast-traveling longitudinal waves (in-plane waves) [4], an SI measurement system must be capable of capturing in-plane vibrations.

Due to these challenges, n o experimental validation has yet been conducted for the FEM-based instantaneous SI analysis proposed by the authors. Therefore, this study aims to establish an instantaneous SI measurement technique by extending the existing finite difference approximation method for steady-state SI measurement to transient first-wave propagation. The target structure is a thin-walled planar structure. First, a rigorous formulation of instantaneous SI incorporating all relevant stress components is derived based on plate theory and expressed in terms of vibration displacement. Next, a time-series vibration displacement measurement method using a laser Doppler vibrometer (LDV) is proposed, and the validity of the obtained data is examined by comparing it with FEM results. Finally, the measured displacement data is applied to the proposed SI approximation method, and the experimental SI values are compared with FEM results to evaluate the effectiveness of the measurement technique and the entire identification process.

2. DETAILS OF THE STUDY

2.1 Evaluation process of instantaneous SI

In this study, SI is identified by considering axial force, bending moment, torsional moment, and shear force acting on a thin plate. The evaluation process follows three major steps, as shown in Figure 1: (1) Formulation, (2) Finite Element Method (FEM) Analysis, and (3) Measurement.

(1) Formulation: The relationship between stress and displacement is formulated based on Timoshenko's plate theory. SI is described using partial differential equations incorporating both time and spatial terms of displacement. The finite difference method (FDM) is employed to discretize these differential terms, leading to an approximate SI expression in terms of displacement at discrete points.

(2) Finite Element Analysis (FEM): To verify the validity of the formulation, discrete displacement data obtained from transient response analysis via FEM are substituted into the approximate SI expression derived in (1). The consistency between this computed SI and the instantaneous SI directly obtained from the FEM analysis (considered as the true value) is then evaluated.

(3) Measurement: The wave propagation is experimentally obtained by applying impact excitation via hammering on a test specimen. To eliminate errors related to time and spatial dependencies in measurement, noise removal and averaging techniques are applied to correct the acquired data. The accuracy of the measurement is assessed by correlating it with FEM analysis results. Finally, the vibration displacement is substituted into the approximate SI equation derived in step (1) to determine the instantaneous SI.

Through this process, the consistency between the approximate and numerical solutions (true values) of instantaneous SI is evaluated to validate the proposed measurement technique and identification process. In the subsequent sections, Chapter 3 presents the formulation and validation of SI approximation accuracy, Chapter 4 discusses wave propagation measurement, and Chapter 5 evaluates the accuracy of instantaneous SI.

2.2 Test specimen

A hollow steel frame and a panel, simulating the floor of an automobile monocoque structure, were joined by spot welding at 33 points along the four edges (Figure 2). The panel dimensions were 558 × 549 mm^2, corresponding to those of a car body, with a thickness of 1.4 mm. The frame was composed of four rectangular-section electric resistance welded (ERW) steel tubes, each with a plate thickness of 1.6 mm. The cross-sectional area was set to approximately 68 × 57 mm^2, equivalent to that of a typical automobile frame.

The butt joints between the members were fully welded around their perimeters and then planed to a flat surface by cutting. To facilitate the use of a resistance welding gun, round holes were drilled on the backside of the frame at the welding points to serve as electrode insertion ports.

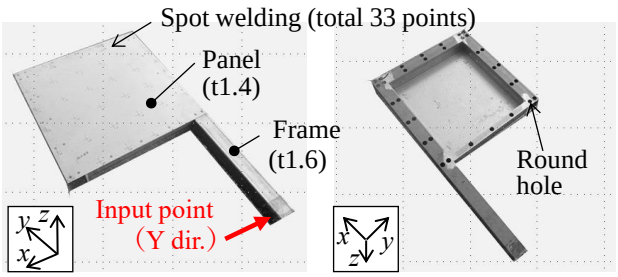

(a) Front side (b) Back side

Figure 2. Test specimen

3. INSTANTANEOUS SI FORMULATION

3.1 Basic theory

Instantaneous SI is defined as the instantaneous value of vibrational energy per unit width passing through the structure. For a thin-walled structure in the *x*-*y* plane, the instantaneous SI vector $I_x^{shell}\ x,y,t$, $I_y^{shell}\ x,y,t$ at position (*x*, *y*), and time *t* for element *i* is expressed as the product of the stress tensor and vibration velocity.

$$\begin{aligned} I_x^{shell}\ x,y,t &= -N_{xx}\frac{\partial \zeta_x}{\partial t} + Q_x\frac{\partial \zeta_z}{\partial t} \\ &\quad - M_{xx}\frac{\partial^2 \zeta_z}{\partial x \partial t} - M_{xy}\frac{\partial^2 \zeta_z}{\partial y \partial t}, \\ I_y^{shell}\ x,y,t &= -N_{yy}\frac{\partial \zeta_y}{\partial t} + Q_y\frac{\partial \zeta_z}{\partial t} \\ &\quad - M_{yy}\frac{\partial^2 \zeta_z}{\partial y \partial t} - M_{yx}\frac{\partial^2 \zeta_z}{\partial x \partial t} \end{aligned} \tag{1}$$

where *x*, *y*, *z* are the spatial coordinates, ζ is the displacement, N_{xx}, N_{yy} are axial forces (in-plane forces) per unit width, Q_x, Q_y are shear forces per unit width, and M_{xx}, M_{yy} are the bending moments per unit width section, and M_{xy}, M_{yx} are torsional moments per unit width section shown in Figure 3. In this study, which focuses on the initial wave propagation occurring immediately after input, SI based on in-plane forces is included in the formulation in addition to out-of-plane forces, as it is necessary to account for longitudinal vibrations with high vibration velocity. The in-plane shear force $N_{xy} = N_{yx}$ is neglected because its magnitude is small.

3.2 Formulation of Instantaneous SI with displacement

Based on the plate theory, each stress component can be expressed in terms of displacement as follows:

$$\begin{aligned} N_{xx} &= \frac{E}{1-\nu^2}\left(\frac{\partial \zeta_x}{\partial x} + \nu\frac{\partial \zeta_y}{\partial y}\right), \\ N_{yy} &= \frac{E}{1-\nu^2}\left(\frac{\partial \zeta_y}{\partial y} + \nu\frac{\partial \zeta_x}{\partial x}\right), \\ M_{xx} &= -B\left(\frac{\partial^2 \zeta_z}{\partial x^2} + \nu\frac{\partial^2 \zeta_z}{\partial y^2}\right), \\ M_{yy} &= -B\left(\frac{\partial^2 \zeta_z}{\partial y^2} + \nu\frac{\partial^2 \zeta_z}{\partial x^2}\right), \\ M_{xy} &= -M_{yx} = -B\ 1-\nu\ \frac{\partial^2 \zeta_z}{\partial x \partial y}, \\ Q_x &= -B\frac{\partial}{\partial x}\ \nabla^2 \zeta_z\ = -B\frac{\partial}{\partial x}\left(\frac{\partial^2 \zeta_z}{\partial x^2} + \frac{\partial^2 \zeta_z}{\partial y^2}\right), \end{aligned} \tag{2}$$

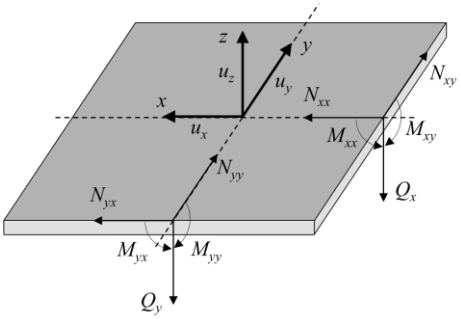

Figure 3. Definition of axis, displacement, force, and moment

$$Q_y = -B\frac{\partial}{\partial y}\ \nabla^2 \zeta_z\ = -B\frac{\partial}{\partial y}\left(\frac{\partial^2 \zeta_z}{\partial x^2} + \frac{\partial^2 \zeta_z}{\partial y^2}\right)$$

where ∇^2 is the two-dimensional Laplacian, E is Young's modulus, and B is the bending stiffness of the plate, given by the following equation using the plate thickness h and Poisson's ratio ν:

$$B = \frac{Eh^3}{12\ 1-\nu^{\ 2}} \tag{3}$$

By substituting equation (2) into equation (1), the instantaneous SI is obtained.

3.3 Derivation of the approximate solution for instantaneous SI using finite difference method (FDM)

the two-dimensional space is discretized into a lattice structure as shown in Figure 4, where the coordinates of a grid point at position $x - y$ and time t are denoted as (x_i, y_j, t_n), and the discrete representation of displacement is expressed as $\zeta_{i,j}^n$. The spatial discretization intervals are defined as Δx in the x direction, Δy in the y direction, and the time discretization interval as Δt . For the finite difference approximation of each derivative term, 12 points surrounding the computation point (red point in the figure) are used (yellow points in the figure). The differential terms are obtained by applying difference operations to the displacement values at these grid points.

The spatial differential term is given by

$$\frac{\partial \zeta}{\partial x} \approx \frac{\zeta_{i+1,j}^n - \zeta_{i-1,j}^n}{2\Delta x} \tag{4}$$

$$\frac{\partial \zeta}{\partial y} \approx \frac{\zeta_{i,j+1}^n - \zeta_{i,j-1}^n}{2\Delta y} \tag{5}$$

$$\frac{\partial^2 \zeta}{\partial x^2} \approx \frac{\zeta_{i+1,j}^n - 2\zeta_{i,j}^n + \zeta_{i-1,j}^n}{\Delta x^2} \tag{6}$$

$$\frac{\partial^2 \zeta}{\partial y^2} \approx \frac{\zeta_{i,j+1}^n - 2\zeta_{i,j}^n + \zeta_{i,j-1}^n}{\Delta y^2} \tag{7}$$

$$\frac{\partial^2 \zeta}{\partial x \partial y} \approx \frac{\zeta_{i+1,j+1}^n - \zeta_{i+1,j-1}^n - \zeta_{i-1,j+1}^n + \zeta_{i-1,j-1}^n}{4\Delta x \Delta y} \tag{8}$$

$$\begin{aligned} \frac{\partial}{\partial x} \nabla^2 \zeta_z &\approx \frac{\nabla^2 \zeta_{i+1,j}^n - \nabla^2 \zeta_{i-1,j}^n}{2\Delta x} \\ &\approx \frac{1}{2\Delta x}\left[\frac{\zeta_{i+2,j}^n - 2\zeta_{i+1,j}^n + \zeta_{i,j}^n}{\Delta x^2}\right. \\ &+ \frac{\zeta_{i+1,j+1}^n - 2\zeta_{i+1,j}^n + \zeta_{i+1,j-1}^n}{\Delta y^2} \\ &- \frac{\zeta_{i,j}^n - 2\zeta_{i-1,j}^n + \zeta_{i-2,j}^n}{\Delta x^2} \\ &\left. - \frac{\zeta_{i-1,j+1}^n - 2\zeta_{i-1,j}^n + \zeta_{i-1,j-1}^n}{\Delta y^2}\right] \end{aligned} \tag{9}$$

$$\begin{aligned} \frac{\partial}{\partial y}(\nabla^2 \zeta_z) &\approx \frac{\nabla^2 \zeta_{i,j+1}^n - \nabla^2 \zeta_{i,j-1}^n}{2\Delta y} \\ &\approx \frac{1}{2\Delta y}\left[\frac{\zeta_{i+1,j+1}^n - 2\zeta_{i,j+1}^n + \zeta_{i-1,j+1}^n}{(\Delta x)^2}\right. \\ &+ \frac{\zeta_{i,j+2}^n - 2\zeta_{i,j+1}^n + \zeta_{i,j}^n}{(\Delta y)^2} \\ &- \frac{\zeta_{i+1,j-1}^n - 2\zeta_{i,j-1}^n + \zeta_{i-1,j-1}^n}{(\Delta x)^2} \\ &\left. - \frac{\zeta_{i,j}^n - 2\zeta_{i,j-1}^n + \zeta_{i,j-2}^n}{(\Delta y)^2}\right] \end{aligned} \tag{10}$$

the time differential term is given by

$$\frac{\partial \zeta}{\partial t} \approx \frac{\zeta_{i,j}^{n+1} - \zeta_{i,j}^{n-1}}{2\Delta t} \tag{11}$$

And the composite differential terms in time and space are given by

$$\frac{\partial^2 \zeta}{\partial x \partial t} \approx \frac{\zeta_{i+1,j}^{n+1} - \zeta_{i-1,j}^{n+1} - \zeta_{i+1,j}^{n-1} + \zeta_{i-1,j}^{n-1}}{4\Delta x \Delta t} \tag{12}$$

$$\frac{\partial^2 \zeta}{\partial y \partial t} \approx \frac{\zeta_{i,j+1}^{n+1} - \zeta_{i,j-1}^{n+1} - \zeta_{i,j+1}^{n-1} + \zeta_{i,j-1}^{n-1}}{4\Delta y \Delta t} \tag{13}$$

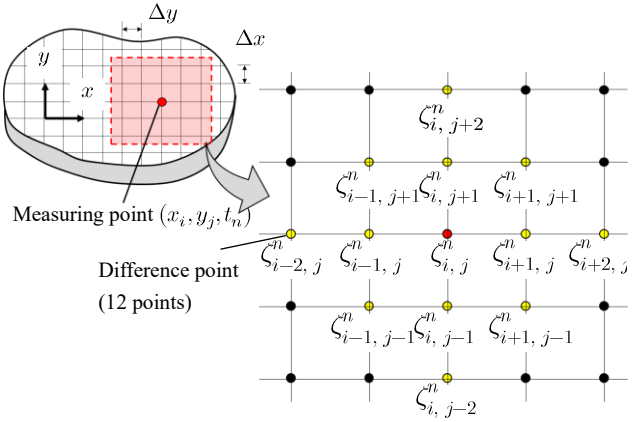

Figure 4. Layout of measurement point and difference point

3.4 Verification of the accuracy of finite difference approximation of instantaneous SI

The accuracy of the instantaneous SI approximation using FDM is validated. If measured values were used for verification, it would be impossible to separate approximation errors from measurement errors. Therefore, FEM analysis results were utilized for this validation. The exact solution of instantaneous SI $\boldsymbol{I}_{ext}$, directly output from transient response analysis, was taken as the true value. The consistency of the approximate solution $\boldsymbol{I}_{apx}$, obtained using FDM based on displacement values from the same FEM analysis, was evaluated.

Figure 5 presents the results at 0.35 ms, the time at which the first wave reaches the panel. To improve the visibility of the energy flow, the vector scale was unified, and the magnitude of the vectors was represented as a contour plot. This visualization method is applied to all subsequent figures. As shown in Figure 5, the vectors generally exhibit good agreement across the entire panel surface. In particular, the accuracy of the approximate solution $\boldsymbol{I}_{apx}$ is ensured in the far-field region of the flat panel, particularly near the center of the panel. On the other hand, the accuracy decreases in the vicinity of discontinuities such as the joint sections between the structural members (dashed areas in the figure). This is attributed to the influence of high-order partial derivative terms—up to the fourth order—used to describe bending moments, torsional moments, and shear forces in the finite difference approximation, resulting in approximation errors [9].

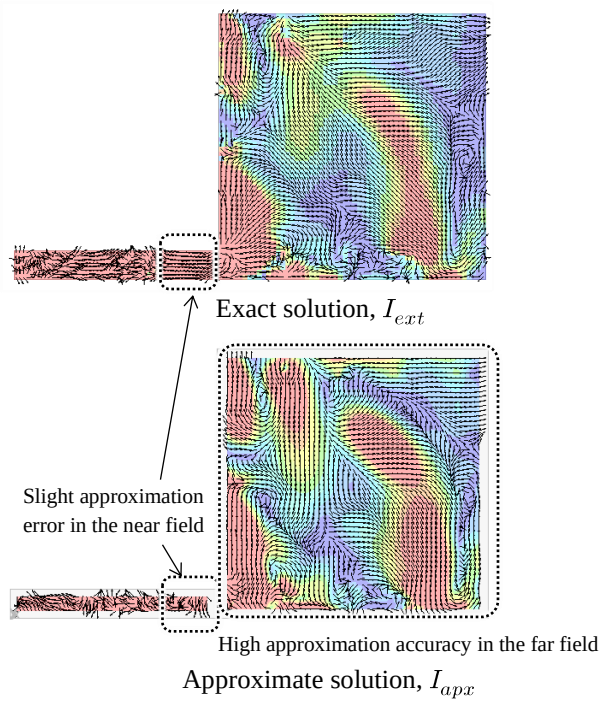

Figure 5. Verification results of finite difference approximation accuracy using FEM (t = 0.35 ms)

4. MEASUREMENT OF WAVE PROPAGATION

To capture the propagation of the wave that occurs immediately after input excitation, the required spatial and temporal resolution was examined, and a suitable measurement method was determined.

4.1 Consideration of measurement resolution

In this study, structure-borne sound is the target phenomenon, and the upper frequency limit for wave observation is set to approximately 1 kHz. Accordingly, the appropriate temporal and spatial resolution was investigated.

The temporal resolution Δt was determined based on the sampling theorem. To prevent aliasing, the sampling frequency is typically set to at least twice the maximum frequency. However, to capture fine temporal variations, a sampling frequency 20 times the maximum frequency—20 kHz—was selected, resulting in a time resolution of 0.05 ms.

Next, the spatial resolution Δx, Δy was considered. The wavelength λ of the wave is given by the relationship between the propagation speed c of the medium and the frequency f: $\lambda = c/f$.

For steel, the wave propagation speed is approximately 5,800 m/s. Thus, the wavelength of a 1 kHz wave is around 3.0 m. In general, wave observation requires a spatial resolution of at most 1/10 of the wavelength [9], which suggests that a theoretical resolution of about 0.3 m would be sufficient. However, to capture the energy flow in greater detail and facilitate a comparison with FEM results, the discretization interval was set to match that of the FEM analysis: 7.5 mm for the frame and 10 mm for the panel. A total of 3,467 measurement points were arranged in an orthogonal grid.

4.2 Measuring equipment

The selection criteria for the measurement equipment were as follows: (a) The ability to meet the previously discussed spatial and temporal resolution requirements. (b) The use of a non-contact sensor to prevent mass loading effects, as the test specimen consists of a thin-walled plate with a thickness of approximately 1–2 mm. (c) The capability to measure not only out-of-plane vibrations but also in-plane vibrations, as the primary wave component of the first wave is longitudinal. To fulfill these requirements and ensure efficient and accurate measurement, a LDV (Polytec PSV-500-3D) was selected. The LDV is a non-contact vibration measurement device that utilizes the Doppler effect of laser light. It operates by detecting frequency shifts in laser light reflected from the measurement surface to determine vibration velocity. This system is equipped with three laser heads, allowing it to geometrically compute and acquire translational vibration velocities in three directions.

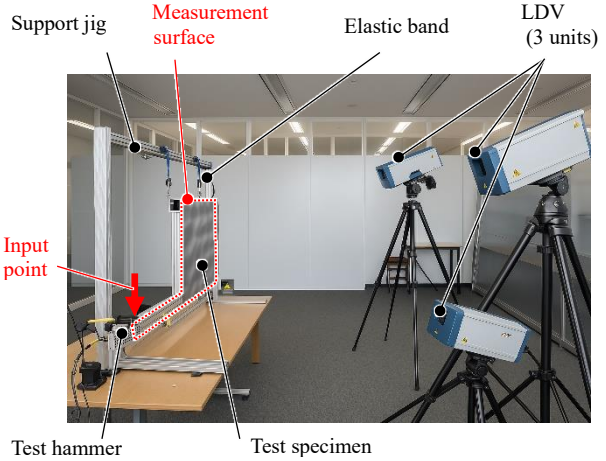

Figure 6. Overview of experimental setup

4.3 Excitation and measurement conditions

An overview of the test is shown in Figure 5. The input method was impact excitation by hammering, with the position at the tip of the frame in the *y*-direction (red arrow in the figure). An automatic modal hammer was used to ensure efficient multi-point measurement and coherent input position and gain at each input point. The boundary condition was a flexible support using elastic bands. The measurement surface was limited to the frontal area indicated by the red dashed line in the figure.

4.4 Elimination of measurement errors and noise associated with data processing

Since the measurement involved scanning laser irradiation at each point, potential errors related to time and spatial resolution were considered. Below, specific sources of error and their mitigation strategies are described.

Temporal errors may arise due to trigger timing misalignment, leading to insufficient time synchronization between measurement points. To address this, hammering was conducted using actuator control, and the trigger signal start time was set based on the excitation cycle to ensure synchronization.

Spatial errors can occur due to misalignment of laser irradiation positions. A primary cause of this misalignment is the minute rotations or translations of the test specimen during repeated excitation trials under soft support conditions. To reduce this error, a Gaussian filter was applied to the measured data. This allowed for local variations in spatial distribution to be reduced by computing each point's value as a weighted average of surrounding points.

Additionally, when integrating the acquired vibration velocity to obtain displacement, the potential superposition of DC noise was a concern. To mitigate this, wavelet transformation was applied to the time-series velocity data obtained from the LDV. Specifically, vibrations before the excitation time were set to zero, and a band-pass filter was applied to the data after excitation to remove noise components.

4.5 Vibration velocity measurement results

The time-series vibration velocity was compared with the transient response analysis results. When setting the excitation time to 0 s, the results at 0.25 ms—when the first wave entered the panel—were visualized (Figure 7). Immediately after excitation, the wave propagated in the elongation direction of the frame and reached the frame joint section before transferring from the frame to the panel. This

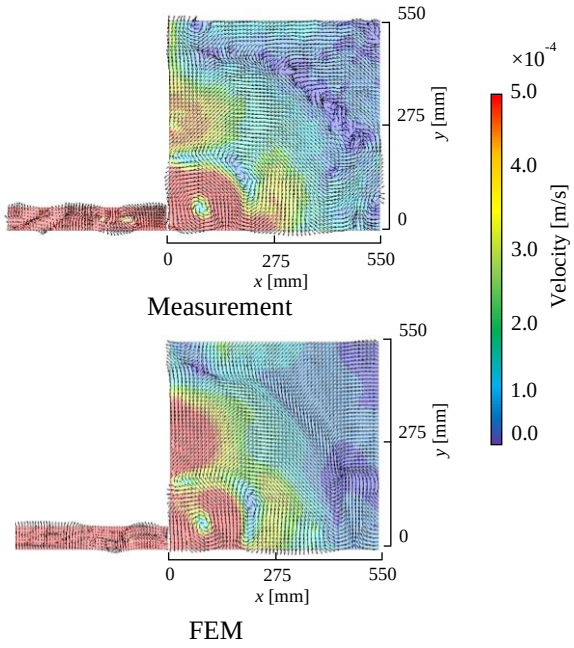

Figure 7. Velocity map at consecutive time samples after impact on a test specimen at 0.25 ms

behavior was accurately matched between the experiment and FEM analysis.

Furthermore, the distance from the frame's end to the joint section was 0.4 m. Given that the theoretical propagation speed in steel is approximately 5,800 m/s, the estimated wave arrival time at the panel was theoretically valid. This confirmed that the measurement had sufficient resolution and accuracy to observe the first-wave propagation.

The LDV-based measurement method was found to be a short-duration and simple process while achieving resolution and precision comparable to FEM. The effectiveness of this approach was thus validated.

5. VERIFICATION OF INSTANTANEOUS STRUCTURAL INTENSITY

The accuracy of the approximate identification of instantaneous SI and the validity of the measurement process were evaluated by comparing the results with FEM analysis.

5.1 Comparison with FEM analysis results

The vibration velocity obtained from LDV was integrated over time to derive displacement. Using finite difference approximation, the instantaneous SI components,

$\boldsymbol{I}_x^{shell}(x,y,t)$ and $\boldsymbol{I}_y^{shell}(x,y,t)$, were computed. Based on these values, the temporal and spatial distributions of vibration energy flow were visualized, and a comparison with FEM analysis—considered the true value—is shown in Figure 8a.

For spatial variation analysis, the SI distribution along section AA (at y = 100 mm) at t = 0.25 ms (the time when the first wave enters the panel) was compared in Figure 8b. Additionally, for temporal variation analysis, the time evolution of SI at point P from t = 0 to 0.35 ms was compared in Figure 8c.

5.2 Consistency Evaluation between Experimental and Numerical Results

As shown in Figure 8a, the vibration energy flow exhibited good consistency between the experiment and FEM analysis in both the inflow region from the frame to the panel and the propagation process within the panel. In particular, the spatial variation of SI at section AA (Figure 8b) demonstrated high quantitative accuracy in both vector direction and magnitude in the central region of the panel, where the influence of near-field waves was minimal.

Furthermore, the time variation of SI at point P (Figure 8c) confirmed the consistency in both the wave arrival time and the temporal evolution of the vector field. On the other hand,

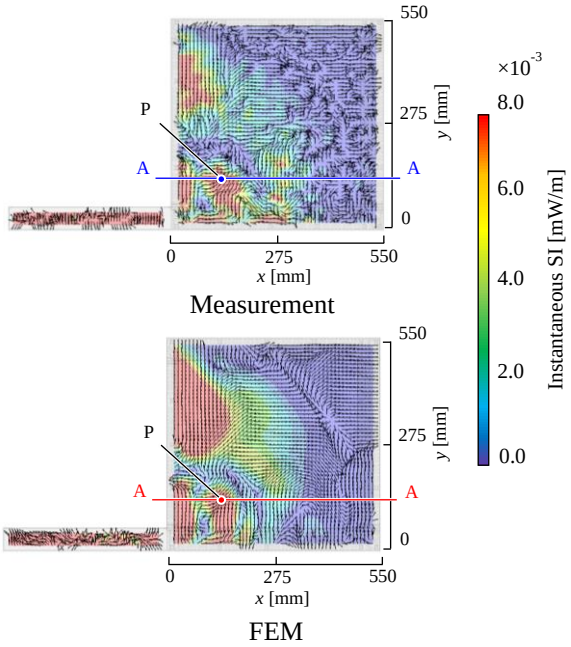

(a) SI map at consecutive time samples after impact on a test specimen at 0.25 ms

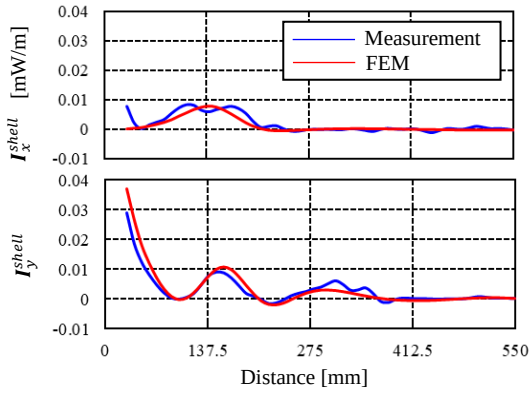

(b) Spatial distribution of structural intensity in the AA cross-section

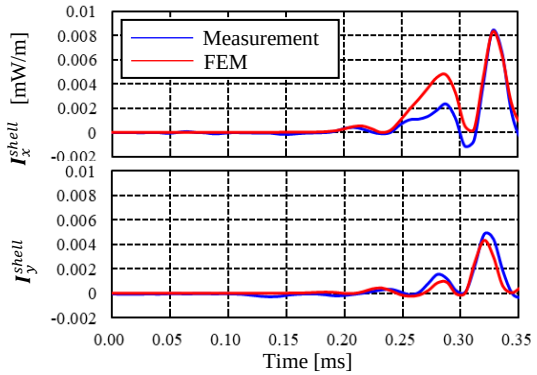

(c) Time history of structural intensity at point P

Figure 8. Verification result of instantaneous SI

vector inconsistencies observed in the panel region at x = 300 to 550 mm were attributed to the noise floor of the measurement system, as the first wave had not yet arrived in this region. This effect was considered negligible.

From these results, the proposed SI formulation, the effectiveness of LDV-based wave propagation measurement, and the validity of the SI approximation process based on the measured data were all confirmed. It was demonstrated that high-accuracy experimental identification of instantaneous SI is achievable.

6. CONCLUSION

This study aimed to evaluate the vibration energy flow of the first wave in an unsteady state through time-series analysis. A measurement method for instantaneous vibration intensity (SI) was examined, and its validity and usefulness were assessed. The key findings are summarized as follows:

(1) Based on plate theory, the exact solution for instantaneous SI was described using a partial

differential equation incorporating temporal and spatial derivatives of vibration displacement. The existing finite difference approximation method was extended to be applicable to the first wave in an unsteady state, and a new approximation formula was proposed.

(2) A non-contact scanning measurement method using LDV was applied to capture the time-series propagation of the first wave in metallic components, and its effectiveness was validated.

(3) The experimentally identified instantaneous SI showed high consistency with FEM analysis in both temporal and spatial variations. This confirmed the validity of the SI identification process, including its formulation and measurement method, establishing a methodology for measuring instantaneous vibration intensity in planar structures.

7. ACKNOWLEDGMENTS

We would like to express our deepest gratitude to Polytec Japan for their cooperation in making the measurements in this study possible.

8. REFERENCES

[1] Noiseux, D.U.: "Measurement of Power Flow in Uniform Beams and Plate", Journal of Acoustical Society of America, Vol.47, pp.238-247, 1970.

[2] Yamazaki, T., "Structural Body and System Design Method based on Vibration Energy Propagation Properties", Journal of Society of Automotive Engineers of Japan, Vol.74, No.7, pp.56-62, 2020.

[3] Abe K., Tanaka Y., Yamazaki T.: "Vibrational Energy Propagation Analysis at Point Joints between Frame and Panel for Vehicle Interior Noise Reduction", *SAE Tech. Paper*, 2024-01-2346, 2024.

[4] W. Dörfler et al.: "*Wave Phenomena: Mathematical Analysis and Numerical Methods*", Birkhäuser, 2023.

[5] Abe K., Tanaka Y., Yamazaki T.: "Instantaneous Structural Intensity Analysis on Vehicle Body", in *Proc. of INTER-NOISE 202*3 (Makuhari, Japan), Vol.268, No.8, pp.619-628, 2023.

[6] G.Pavić: "Measurement of structure borne wave intensity", Part1, *Journal of Sound and Vibration*, Vol.49, No.2, pp.221-230, 1976.

[7] Yamazaki T., Structural Vibration Analysis Using Structural Intensity Measurement, Transactions of the Japan Society of Mechanical Engineers, Vol.65, Issue 633, pp.1772-1777, 1999.

[8] Kamata M., A Study on Structural Intensity Measurement: 2nd Report: Experimental Investigation, Transactions of the Japan Society of Mechanical Engineers, Vol.57, Issue 536, pp.1196-1201, 1991.

[9] Kamata M., A Study on Structural Intensity Measurement: 4th Report, Investigation of Two-Dimensional Structural Intensity, Transactions of the Japan Society of Mechanical Engineers, Vol.62, Issue 594, pp.451-458, 1996.